Available online at www.sciencedirect.com
SCIENCE DIRECT®
PERGAMON
International Journal of Heat and Mass Transfer 47 (2004) 43–61
International Journal of HEAT and MASS TRANSFER
www.elsevier.com/locate/ijhmt

Effects of a first-order chemical reaction on turbulent mass transfer

Bojan M. Mitrovic [a], Dimitrios V. Papavassiliou [a,b,*]

[a] School of Chemical Engineering and Materials Science, The University of Oklahoma, 100 East Boyd St., Sec T335, Norman, OK 73019, USA

[b] Sarkeys Energy Center, The University of Oklahoma, 100 East Boyd, Norman, OK 73019 USA

Received 7 March 2003; received in revised form 18 June 2003

Abstract

The effects of a first-order chemical reaction on turbulent mass transfer from a wall are investigated using a Lagrangian method that involves the numerical solution for the flow field in conjunction with the tracking of mass markers released from the wall. The markers react according to a Poisson distribution that is correlated to the reaction rate constant. The method allows studying a range of Schmidt number fluids and a range of Damköhler numbers. The behavior of a continuous line source of the reactant, and the behavior of the dissolution of the reactant from the wall are examined. It is found that the mass transfer coefficient increases dramatically when a first-order reaction occurs. A correlation between the mass transfer coefficient and the Damköhler number is proposed for both low and high Schmidt numbers. The fundamental reason for the change in the mass transfer properties is that each marker is affected by different parts of the turbulence velocity field depending on the Schmidt and Damköhler numbers.
© 2003 Elsevier Ltd. All rights reserved.

1. Introduction

Several industrial processes involve chemical reactions in turbulent flows [1]. Understanding the effect of turbulence structure on chemical reaction kinetics (and the reverse) is still an open question, one that is important from a theoretical standpoint, and for the development of models based on flow characteristics. The inclusion of chemical reactions in a turbulence simulation presents more difficulties than the addition of conservation equations for chemical species [2], and state-of-the art commercial simulations for chemically reacting flows use closure models [2,3]. Direct numerical simulations (DNS) that do not utilize empirical correlations have been used to describe mainly isotropic turbulence cases [1,4].

In this work, a Lagrangian method is applied to the case of first-order chemical reaction. Typical examples of first-order reactions are isomerization reactions, radioactive decay, and biodegradation. The basic concept is that mass markers (reactant) are released in a turbulent field generated by a DNS and transformed to a product later in time, using a probability function that depends on the reaction rate coefficient. Concentration profiles are generated and the effect of the reaction on the mass transfer coefficient is explored. The findings of this paper include: (a) the mass transfer coefficient increases dramatically when a first-order reaction occurs, as has been found previously [5,6]; (b) the reason for the dependence of mass transfer properties on *Sc* is that each marker is affected by different parts of the turbulence velocity field depending on the *Sc*; and (c) a correlation between mass transfer coefficient and Damköhler number.

2. Lagrangian scalar tracking methodology

The basic concept of Lagrangian scalar tracking (LST) is that passive scalar transport from the wall in

* Corresponding author. Address: School of Chemical Engineering and Materials Science, The University of Oklahoma, 100 East Boyd St., Sec T335, Norman, OK 73019, USA. Tel.: +1-405-325-0574; fax: +1-405-325-5813.

E-mail address: dvpapava@ou.edu (D.V. Papavassiliou).

0017-9310/$ - see front matter © 2003 Elsevier Ltd. All rights reserved.
doi:10.1016/S0017-9310(03)00380-6

Nomenclature

C	concentration
c'	concentration fluctuation
D	molecular diffusivity
Da	Damköhler number
h	half-height of the channel
J_w	mass flux from the wall
K	mass transfer coefficient
K_∞	mass transfer coefficient for a fully developed turbulent flow
k_{A1}	reaction rate constant
l^*	characteristic length scale, $l^* = \nu/u^*$
N_A, N_B	number of markers A and B
P_1	conditional probability for a marker to be at a location (x, y) at time t, given that it was released at a known time from a known location at the wall
P_2	joint probability for a marker to be at a location (x, y)
Pr	Prandtl number, $Pr = \nu/\alpha$
q^2	turbulent kinetic energy
R	duct radius
Re	Reynolds number, $Re = U_c h/\nu$
r_A	rate of reaction
Sc	Schmidt number, $Sc = \nu/D$
t	time
$t_{1/2}$	half-life time for a first-order reaction
t^*	characteristic time scale, $t^* = \nu/(u^*)^2$, $t^* = 1$ for the DNS
$\vec{U}$	Eulerian velocity vector
u^*	friction velocity, $u^* = (\tau_w/\rho)^{1/2}$
u', v', w'	root mean square of the fluctuating velocity in the x, y, z directions (in wall units)
$\vec{V}$	Lagrangian velocity vector of a marker
x, y, z	streamwise, normal and spanwise coordinates
X	displacement of a marker from the source in the x direction
$\overline{X^2}$	mean-squared particle displacement in the streamwise direction
$\vec{X}$	position vector of a marker

Greek symbols

α	parameter in the model for the mass transfer enhancement factor, $\alpha = 106.46 Da \cdot Sc^{1/3}$
γ	dimensionless rate of reaction for first-order reactions, $\gamma = k_{A1} R^2/\nu$
δ_y	plume half-width
Δt	time step
Δx, Δy	bin size in x, y direction
ε	rate of viscous dissipation per unit mass
λ	characteristic parameter for the Poisson distribution
ν	kinematic viscosity
σ	standard deviation of a probability density function
ϕ	mass transfer coefficient enhancement factor, K(reaction)/K(no reaction)

Superscripts and subscripts

$\overline{()}$	ensemble average
$\vec{()}$	vector quantity
$()^+$	value made dimensionless with the wall parameters
$()^*$	friction value
$()_A$	value related to reactant A
$()_b$	bulk value
$()_{max}$	maximum value
$()_0$	value at the instant of marker release
$()_w$	value at the wall of the channel

turbulent flow is the result of the combined behavior of an infinite number of continuous sources of heat or mass markers, such as the markers discussed by Saffman [7]. Hanratty [8] used this concept to describe the transfer of heat from a hot to a cold wall in turbulent channel flow. Due to the difficulties of conducting laboratory experiments that can measure the trajectories of individual scalar markers in a flow field, the study of heat or mass transfer using these concepts has become feasible with the appearance of supercomputers. Papavassiliou and Hanratty [9,10] used a DNS in conjunction with the tracking of scalar markers to study heat transfer based on direct calculations of the behavior of such wall sources. Details about the implementation and validation of the LST methodology that includes the stochastic tracking of heat or mass markers in a turbulent flow field, and the statistical post-processing of the results to obtain scalar profiles, can be found elsewhere [9–14]. A brief description of the method is included here.

The behavior of a wall source is determined by following the paths of a large number of scalar markers in a flow field created by a DNS. The flow, which is driven by a constant mean pressure gradient in a channel, is for an incompressible Newtonian fluid with constant physical properties. The Reynolds number defined with the centerline mean velocity and the half-height of the channel is 2660. The Reynolds number defined with the centerline mean velocity and the hydraulic diameter of the channel (i.e., equivalent to the Re definition for pipe flow) is 10,640, which falls well into the turbulent flow regime.

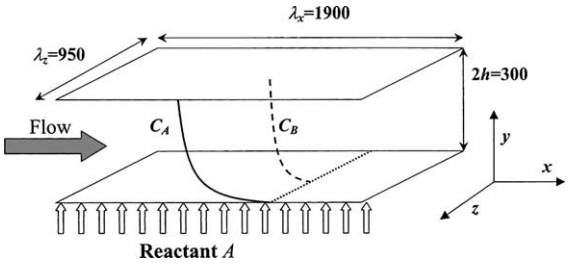

Fig. 1. Computational domain and flow configuration. The concentration profiles are qualitatively sketched (see Fig. 10 for quantitative profiles).

The simulation is conducted on a $128 \times 65 \times 128$ grid in x, y, z. The dimensions of the computational box are $4\pi h \times 2h \times 2\pi h$, where $h = 150$ in wall units. The flow is regarded as periodic in the x and z directions, with the periodicity lengths equal to the dimensions of the computational box in these directions. The configuration of the computational domain is shown in Fig. 1. Since the flow field that results form the DNS is important for the mass transfer calculations that follow, we present here first and second-order turbulence statistics. The mean velocity profile is shown in Fig. 2(a), and the turbulence intensities are shown in Fig. 2(b) for the x, y, and z directions. For more details regarding the statistics of the velocity field, and for the validation of the DNS with experiments, we refer interested readers to [15,16].

A tracking algorithm is used to monitor the space/time trajectories of the markers [17]; their motion is decomposed into a convective part and a molecular diffusion part. The convective part can be calculated from the fluid velocity at the particle position yielding for the equation of particle motion $\vec{V}(\vec{x}_0, t) = \frac{\partial \vec{X}(\vec{x}_0, t)}{\partial t}$, where the Lagrangian velocity of a marker released at location $\vec{x}_0$ is given as $\vec{V}(\vec{x}_0, t) = \vec{U}[\vec{X}(\vec{x}_0, t), t]$ ($\vec{U}$ is the Eulerian velocity of the fluid at the location of the marker at time t).

The effect of molecular diffusion follows from Einstein's theory for Brownian motion [18], which relates the rate of molecular dispersion in a laminar field to the molecular diffusivity $\mathrm{d}\overline{X^2}/\mathrm{d}t = 2D$. The diffusion effect is simulated by superimposing a 3D random walk on the particle motion (which already appears to be random due to turbulence). The size of the random walk takes values from a Gaussian distribution with zero mean and a standard deviation that depends on the Sc of the fluid. The random walk is added on the convective part of the motion after each time step and the standard deviation is $\sigma = \sqrt{2\Delta t/Sc}$ in wall units. Thus, effects of Sc on the process can be studied by modifying σ. If a marker position is found to be inside the channel wall, the marker is reflected symmetrically back into the channel enforcing the boundary condition of an impermeable wall [19]. In addition, the markers are assumed to be passive and, thus, have no effect on the flow.

In this work, two sets of data were considered. These two sets correspond to numerical experiments C and E, as designated in the Lagrangian database of Mitrovic et al. [20]. The typical procedure was to follow markers for several Sc using the same hydrodynamic field. For experiment C a total of 16,129 markers were released instantaneously from a uniform 127×127 rectangular grid that covered the bottom wall of the channel and $Sc = 200$, 2400, 7000, 15,000, and 50,000. The markers were tracked up to the time at which the resulting cloud was distributed uniformly across the channel. The velocities and positions of these markers were stored at every wall time unit for statistical post-processing. Tracking experiment E was conducted by following a total of 145,161 instantaneously released markers from a uniform 381×381 rectangular grid at the bottom wall of the channel and $Sc = 0.1$, 0.7, 6, 10, and 100. The time

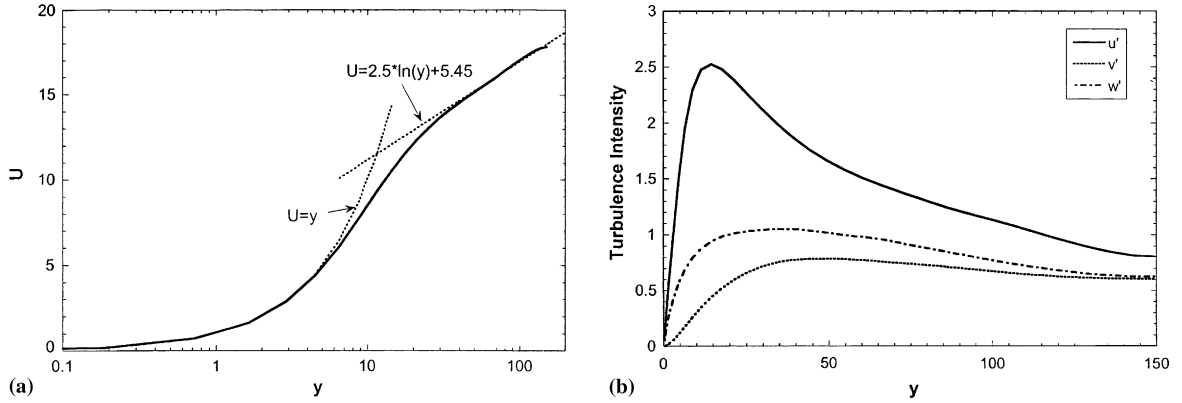

Fig. 2. Turbulent flow statistics for the velocity field: (a) mean velocity profile and (b) turbulence intensity in the streamwise, normal and spanwise flow directions.

step for both the hydrodynamics simulation and the marker tracking was $\Delta t = 0.25$.

3. Synthesis of mean concentration profiles

The building block for the Lagrangian formulation is the behavior of an instantaneous line source of markers located at the wall of the channel. For each numerical experiment, the trajectories of all markers were used as an ensemble to obtain the probability $P_1(x - x_0, y, t - t_0 \,|\, t_0, x_0)$, which represents the joint and conditional probability density function for a marker to be at a location (x, y) at time t, given that the marker was released at x_0 at time t_0. This probability can be interpreted physically as concentration [21] and, thus, as a snapshot of a cloud of contaminants (a puff) released instantaneously from $x_0 = 0$. Integrating probability P_1 over time generates the behavior of a continuous line source at x_0

$$P_2(x - x_0, y \,|\, t_0, x_0) = \int_{t_0}^{\infty} P_1(x - x_0, y, t - t_0 | t_0, x_0)\,\mathrm{d}t \quad (1)$$

Probability P_2 was calculated for each Sc using a grid that covered the flow domain and counting the number of markers that were present in each grid-cell. The grid in the normal direction was constructed either by dividing the width of the channel uniformly in 300 bins ($Sc \leqslant 100$), or by using Chebyshev collocation points to generate 300 bins ($200 \leqslant Sc \leqslant 2400$), or 400 bins ($Sc > 2400$) in order to increase the resolution closer to the wall. The reason for using grids with more bins closer to the wall as Sc increases is that we need to capture several bins within the diffusive wall sublayer, which becomes thinner as Sc increases. For example, this thickness is 0.326 in wall units for $Sc = 50,000$ (according to the suggestion of Kader [22] that the thickness of the diffusive wall sublayer is about $12/Sc$ for $Sc \gg 1$). Using 400 total bins, eight of them lay within the diffusive wall sublayer for $Sc = 50,000$. In the streamwise direction, the grid was stretched, following the relation $\Delta x_n = 1.06^n \Delta x_{(n-1)}$ with $\Delta x_0 = 5$ in wall units. The average number of markers in a bin was 11,520 and 13,820 for the case of numerical experiments C and E, respectively. Papavassiliou [23] has studied the effects of Pr on P_1 and on the evolution of the marker cloud for $0.1 \leqslant Pr \leqslant 50{,}000$, and Mitrovic and Papavassiliou [14] have calculated the turbulent transport properties for the plume that results from a continuous line source, and modeled P_2 for $0.1 \leqslant Pr \leqslant 50{,}000$.

The mass transfer from a dissolving wall was described with a series of continuous line sources covering the wall. The mean concentration profile in a channel, where a mass flux is introduced from the bottom wall at a constant rate (isoflux condition), can be synthesized from P_2 by integrating P_2 over the streamwise direction [12]

$$\begin{aligned}\overline{C}(y) &= \int_{x_0}^{\infty} P_2(x - x_0, y | x_0) \\ &= \int_{x_0}^{\infty}\int_{t_0}^{\infty} P_1(x - x_0, y, t - t_0 | t_0, x_0)\,\mathrm{d}t\,\mathrm{d}x \end{aligned} \quad (2)$$

Similarly, the mean concentration profile at distance $(x_1 - x_0)$ downstream from a step change in wall flux at x_0 can be also synthesized from P_2 as follows:

$$\begin{aligned}\overline{C}(x_1, y) &= \int_{x_0}^{x_1} P_2(x - x_0, y | x_0) \\ &= \int_{x_0}^{x_1}\int_{t_0}^{\infty} P_1(x - x_0, y, t - t_0 | t_0, x_0)\,\mathrm{d}t\,\mathrm{d}x \end{aligned} \quad (3)$$

4. Turbulent transport of heat and mass in an Eulerian framework

In an Eulerian description of turbulent transport, the concentration is decomposed as $C = \overline{C} + c'$. The concentration is usually made dimensionless by using the friction concentration $C^* = J_w/u^*$, where J_w is the mass flux at the wall defined in terms of the diffusivity of the fluid as

$$J_w = -D\left(\frac{\mathrm{d}\overline{C}}{\mathrm{d}y}\right)_w \quad (4)$$

The dimensionless concentration in wall units, C^+, is then defined as

$$C^+ = \frac{C}{C^*} = -\frac{Cu^*}{\left(D\dfrac{\mathrm{d}\overline{C}}{\mathrm{d}y}\right)_w} = -Sc\frac{C}{\left(\dfrac{\mathrm{d}\overline{C}}{\mathrm{d}y^+}\right)_w}, \quad (5)$$

where y^+ is the distance from the wall in viscous wall units ($y^+ = yu^*/\nu$). A dimensionless mass transfer coefficient can be defined as $K^+ = K/u^*$ with K given by the relation

$$J_w = K(\overline{C_b} - \overline{C_w}). \quad (6)$$

The above equations and definitions can be used to derive the following relation:

$$K^+ = \frac{1}{Sc}\left[\frac{d\left[\overline{C}/\left(\overline{C_b} - \overline{C_w}\right)\right]}{\mathrm{d}y^+}\right]_w \quad (7)$$

Mitrovic et al. [20] obtained the following limiting expressions for the mass transfer coefficient for fully developed flow using a consistent set of LST results for different Sc fluids:

$$K_\infty^+ = 0.0465 \cdot Sc^{-0.510} \quad \text{for } Sc \leqslant 10 \quad (8a)$$

$$K_\infty^+ = 0.0835 \cdot Sc^{-0.690} \quad \text{for } Sc \geqslant 100 \quad (8b)$$

Eq. (8b) is in close agreement with the experimental measurements of Shaw and Hanratty [24] that suggested $K^+ \sim Sc^{-0.704}$ and with the theoretical result of Petty [25] that predicted $K^+ \sim Sc^{-0.7}$. The value of the exponent for high Sc dependence is relevant to the fundamental issue of the asymptotic behavior of the eddy diffusivity very close to the wall. At high Sc, the diffusive wall sublayer is thinner than the viscous wall sublayer, so that the velocity field in it can be described using a Taylor series expansion in terms of the distance from the wall. The analogy between momentum transfer and mass or heat transfer suggests that the root mean square of the concentration or temperature fluctuations should change with the velocity fluctuations in the streamwise direction, which means that c'^+ changes with y^+, as $y^+ \to 0$. The root mean square of the velocity fluctuations in the normal direction changes with $(y^+)^2$, as $y^+ \to 0$, and the root mean square of the velocity fluctuations in the streamwise direction changes with y^+, as $y^+ \to 0$ [26]. Based on the definition of eddy diffusivity and the above discussion, the eddy diffusivity should be a power function of the distance from the wall. Son and Hanratty [27] have shown that if it changes with $(y^+)^3$ as $y^+ \to 0$, then $K^+ \sim Sc^{-2/3}$ but if the eddy diffusivity changes with $(y^+)^4$ as $y^+ \to 0$, then $K^+ \sim Sc^{-3/4}$, respectively. The value of the exponent that results from Eq. (8b) is 3.23. For heat transfer (i.e., when the highest Pr hardly ever goes over 100) the value of the exponent can be taken as −2/3 [28].

5. Simulation of a first-order chemical reaction with LST

The specific problem studied here is the isothermal, irreversible, first-order reaction

$$A \to B$$

The rate of reaction, r_A, for the above equation is

$$-r_A = k_{A1} C_A \tag{9}$$

The assumption is made that the number of reactant particles that react and transform to B in every discrete time step, N_{Ar}, follow the Poisson distribution. The Poisson distribution is most commonly used to model the number of random occurrences of some phenomenon within a specified time interval [29]. A Poisson probability function is given by the formula

$$P(X = x) = \frac{\lambda^x e^{-\lambda}}{x!}, \quad x = 0, 1, \ldots \tag{10}$$

where λ is the average number of occurrences within the specified interval, which, in the case of a reaction, can be related to the rate constant k_{A1}. The choice of the Poisson distribution is justified because N_{Ar} satisfies the conditions for an approximate Poisson distribution [29]: (a) the number of reacting particles in non-overlapping time intervals is statistically independent, and (b) the probability of two or more reactions in a sufficiently short interval is essentially zero. The correlation of λ to k_{A1} can be determined from the characteristics of the Poisson distribution; the probability of only one reaction in a sufficiently short time interval Δt is $\lambda \Delta t$ (note that k_{A1} has units of inverse time as does λ, so that $\lambda \Delta t \sim k_{A1} \Delta t$ and $\lambda \sim k_{A1}$). For every time step, it is therefore possible to calculate how many of the remaining A particles will react.

The characteristic time scale for a first-order reaction is the half-life time, which can be determined by rewriting Eq. (9) as $-dC_A/dt = k_{A1} C_A$ and integrating to yield

$$-\ln C_A = k_{A1} + C_1 \tag{11}$$

where C_1 is a constant of integration. If C_{A0} is the concentration of reactant A at zero time (or number of A particles at $t = 0$), then the dimensionless concentration can be expressed as $C_A/C_{A0} = \exp(-k_{A1} t)$. The half-life is the time for one half of the initial number of particles A to react, so

$$C_A/C_{A0} = 1/2 = \exp(-k_{A1} t) \tag{12}$$

resulting into

$$t_{1/2} = 1/k_{A1} \ln 2 = 0.693/k_{A1} \tag{13}$$

The focus of the present work is on rather slow reactions, which allow the development of the concentration field outside the viscous wall region (i.e., those with $t_{1/2} \gg t^*$). In addition to the viscous time scale, another time scale of interest is $t_{1/2} \approx (q^2/\varepsilon)_{max}$ where q^2 is the turbulent kinetic energy and ε is the dissipation at the distance from the wall at which turbulent production is maximum. Seven different values of the half-life time are explored in this work: $t_{1/2} = 50$, $t_{1/2} = 100$, $t_{1/2} = 250$, $t_{1/2} = 500$, $t_{1/2} = 1000$, $t_{1/2} = 2500$ and $t_{1/2} = 5000$. The characteristic parameter for the Poisson distribution can then be found from Eq. (13) as

$$\lambda = k_{A1} = 0.693/t_{1/2} \tag{14}$$

The Damköhler number, Da, which is a measure of the reaction time scale versus the turbulence time scale, is given by

$$Da = \frac{k_n C^{n-1}}{(u/l^*)} = k_n C^{n-1} t^* \tag{15}$$

where k_n is the kinetic reaction coefficient for an nth-order reaction. Therefore, for a first-order reaction

$$Da = k_{A1} t^*, \tag{16}$$

and in the case where the time scale is defined as $(q^2/\varepsilon)_{max}$

$$Da = k_{A1} (q^2/\varepsilon)_{max} \tag{17}$$

Table 1
Rate constants and Damköhler numbers for different values of the half-life time

$t_{1/2}$	k_{A1} or λ	*Da* (Eq. (16))	*Da* (Eq. (17))
50	1.39×10^{-2}	1.39×10^{-2}	2.54×10^{-2}
100	6.93×10^{-3}	6.93×10^{-3}	1.27×10^{-2}
250	2.77×10^{-3}	2.77×10^{-3}	5.08×10^{-3}
500	1.39×10^{-3}	1.39×10^{-3}	2.54×10^{-3}
1000	6.93×10^{-4}	6.93×10^{-4}	1.27×10^{-3}
2500	2.77×10^{-4}	2.77×10^{-4}	5.08×10^{-4}
5000	1.39×10^{-4}	1.39×10^{-4}	2.54×10^{-4}

Table 1 summarizes the calculated values for k_{A1} and *Da* for different values of $t_{1/2}$. For example, if $t_{1/2} = 500$ then $\lambda = 1.386 \times 10^{-3}$, and the probability of each mass marker A not to transform to B in every discrete time step is according to Eq. (10), $P(X = 0) = (1.386 \times 10^{-3})^0 e^{-1.386\times10^{-3}} = 0.9986$. Thus, the probability that a reactant marker A will become B within a time step is $P(X > 0) = 1 - P(X = 0) = 1.4 \times 10^{-3}$. By generating random numbers between 0 and 1 for each reactant and for each time step, and comparing to the above probability, it can be determined how many markers A will transform to B in every Δt.

Results for the case of an instantaneous line source at the wall are compared with the theoretical prediction for the decay of C_A with time (Eq. (12)). The dimensionless concentration for the case of an ensemble of 16,129 instantaneously released mass markers is calculated by dividing the number of the remaining A markers at each time step by the initial number of markers, $N_A(t)/N_{A0}$. Fig. 3 shows a comparison between the theoretical results and the results from the simulation for different values of $t_{1/2}$, where k_{A1} and λ are calculated according to Eq. (14). It is seen that the agreement is very good for all cases signifying the validity of selecting the Poisson distribution. Validation of the results has also been obtained by comparing the mean displacement of markers A and B in the streamwise and the normal direction. Since each marker A has the same probability to become B at any location in the channel, it is expected that the mean displacements in the x and y directions are equal for both marker cloud A and marker cloud B. This prediction has been confirmed for different *Sc*.

6. Results and discussion

6.1. Continuous line source at the wall

Fig. 4(a) and (b) shows the fully developed plume for species A (plume A) and B (plume B), respectively, that are characterized by $Sc = 0.7$ and $t_{1/2} = 500$. It can be seen that plume B stretches much farther downstream from the source than plume A, because species A decays as it moves downstream, and eventually almost all markers A are transformed into B. However, for a slower reaction ($t_{1/2} = 1000$) as seen in Fig. 4(c) and (d), the spread of plume A in the x direction is much closer to the spread of plume B, since fewer of the A markers are transformed with time. Similar behavior is observed for the $Sc = 100$ plumes, as presented in Fig. 5(a)–(b) and (c)–(d) for $t_{1/2} = 500$ and $t_{1/2} = 1000$, respectively. The

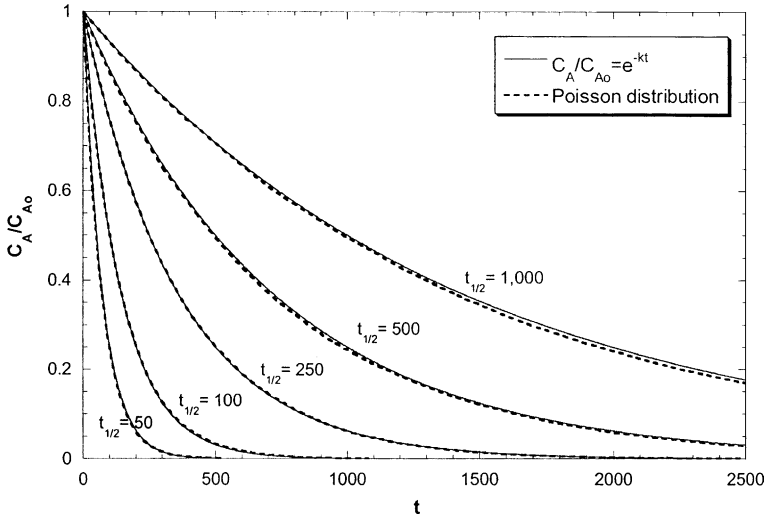

Fig. 3. Comparison between the theoretical prediction for the decay of concentration C_A and LST results obtained with the Poisson distribution for different half-life times.

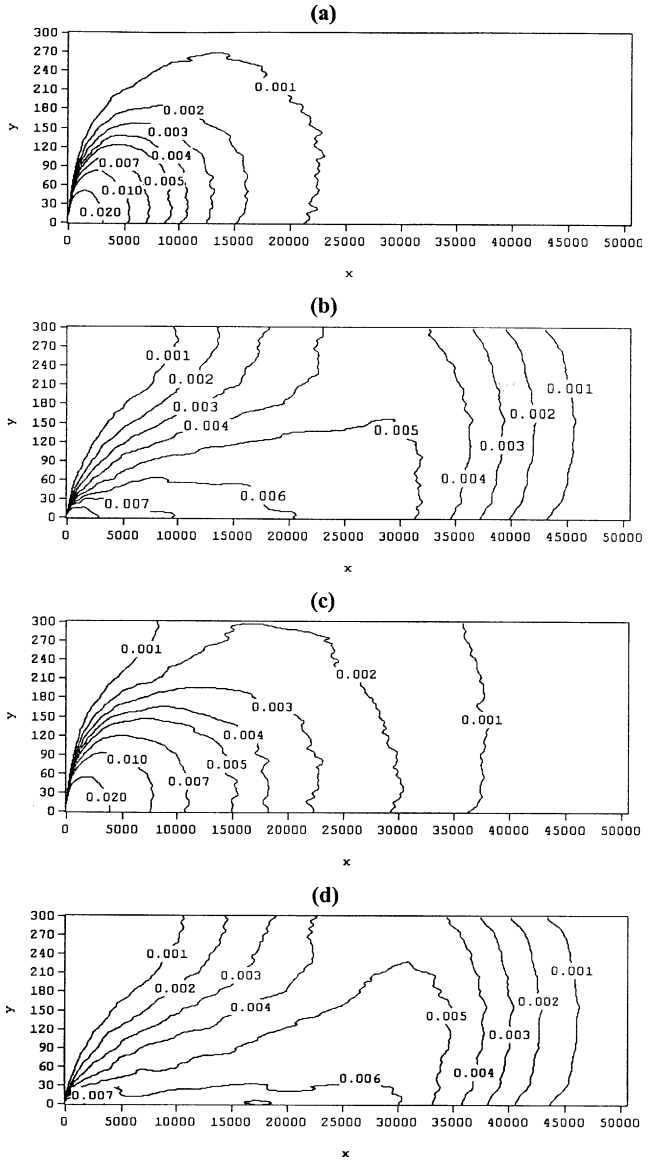

Fig. 4. Fully developed plume for $Sc = 0.7$: (a) reactant A and $t_{1/2} = 500$; (b) product B and $t_{1/2} = 500$; (c) reactant A and $t_{1/2} = 1000$ and (d) product B and $t_{1/2} = 1000$.

effect of Sc on plume development can also be observed, since both plume A and plume B are more dispersed in the channel for $Sc = 0.7$ than the corresponding plumes for $Sc = 100$. It is also shown for both values of $t_{1/2}$ that plume A is characterized by higher concentration close to the source, and by higher concentration gradients, compared with plume B. Such behavior can be interpreted when the stages of plume development identified by Mitrovic and Papavassiliou [14] are taken into account. Markers B spend much longer time in the second stage of plume development (corresponding to the transition stage, where markers get away from the viscous wall subregion and into the outer region) than markers A. Markers A react and change to B mostly within the first stage of plume development, corresponding to the period that the markers are inside the viscous wall subregion.

Fig. 6(a) and (b) presents the half-plume width (i.e., the distance from the wall at which the concentration falls to half its maximum) for $Sc = 0.7$ and $Sc = 100$,

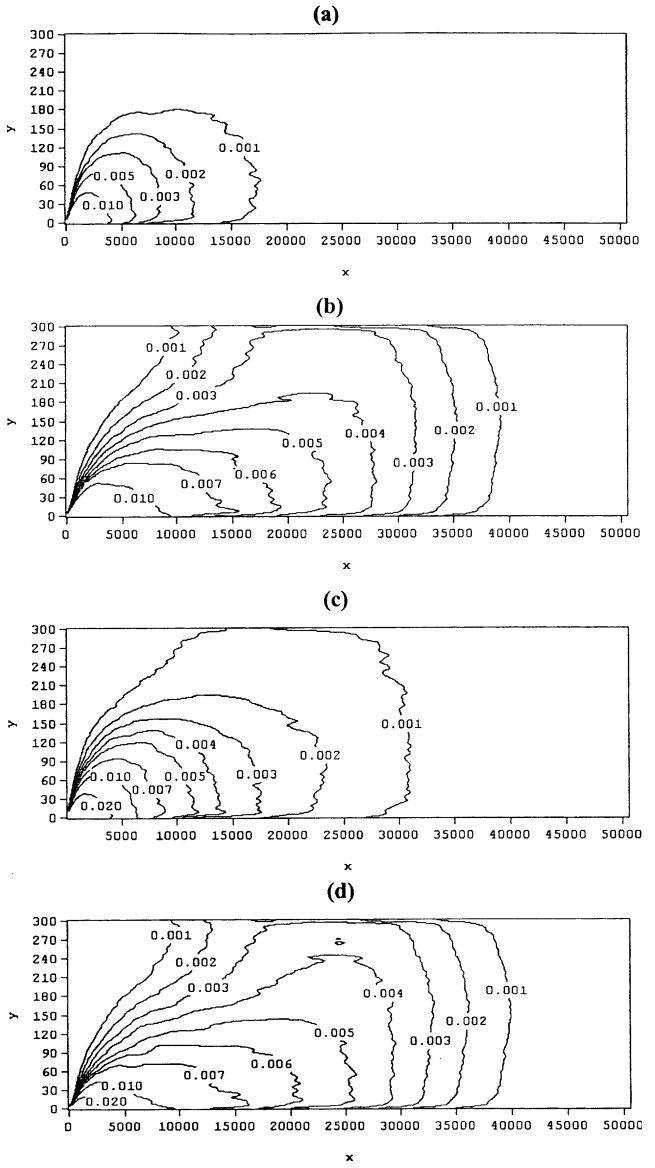

Fig. 5. Fully developed plume for $Sc = 100$: (a) reactant A and $t_{1/2} = 500$; (b) product B and $t_{1/2} = 500$; (c) reactant A and $t_{1/2} = 1000$ and (d) product B and $t_{1/2} = 1000$.

respectively, for a reaction characterized by $t_{1/2} = 500$. It can be seen that δ_y for reactant A is always higher downstream from the source than δ_y for product B. This should be expected, because markers B can be generated only at locations where markers A already exist, and, in this sense, plume B is enclosed by plume A. For $Sc = 100$, the difference is more pronounced. In that case, relatively more markers A stay inside the viscous wall region, markers B are mostly generated within that region, and the leaking process from the wall region to the outer region of the flow for markers B takes longer to develop.

Fig. 7(a) and (b) shows the Sc effect on δ_y for plumes A and B, respectively, for the case of $t_{1/2} = 500$. As Sc increases, it is more difficult for the markers to leave the near wall region because of small molecular jumps and low mean velocities, so the extent of the plumes in the normal direction is smaller. Fig. 8(a)–(c) presents the decay of the ground-level concentration $C_{\max}$ of A and B downstream from a continuous source for $Sc = 0.7$, 100,

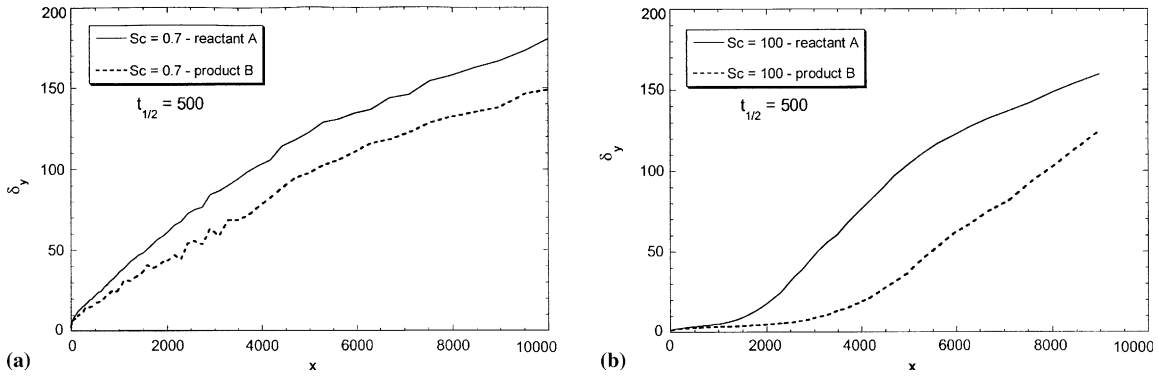

Fig. 6. Half-plume widths of components A and B for $t_{1/2} = 500$: (a) $Sc = 0.7$ and (b) $Sc = 100$.

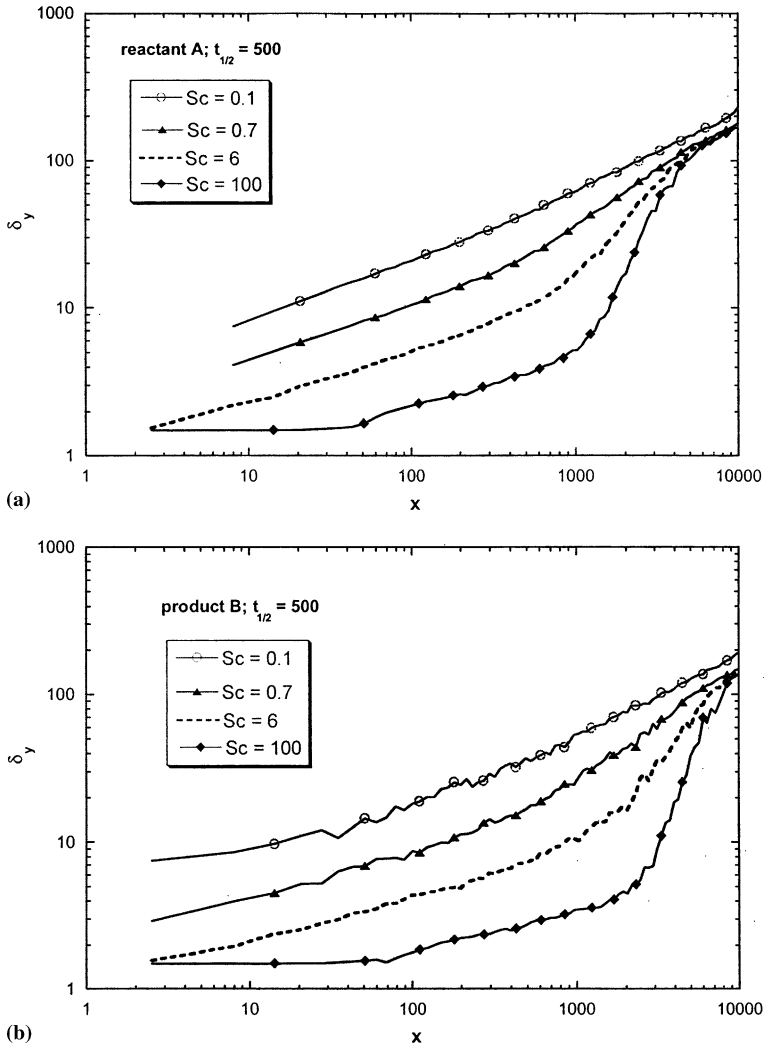

Fig. 7. Half-plume widths for $t_{1/2} = 500$ and different Sc: (a) reactant A and (b) product B.

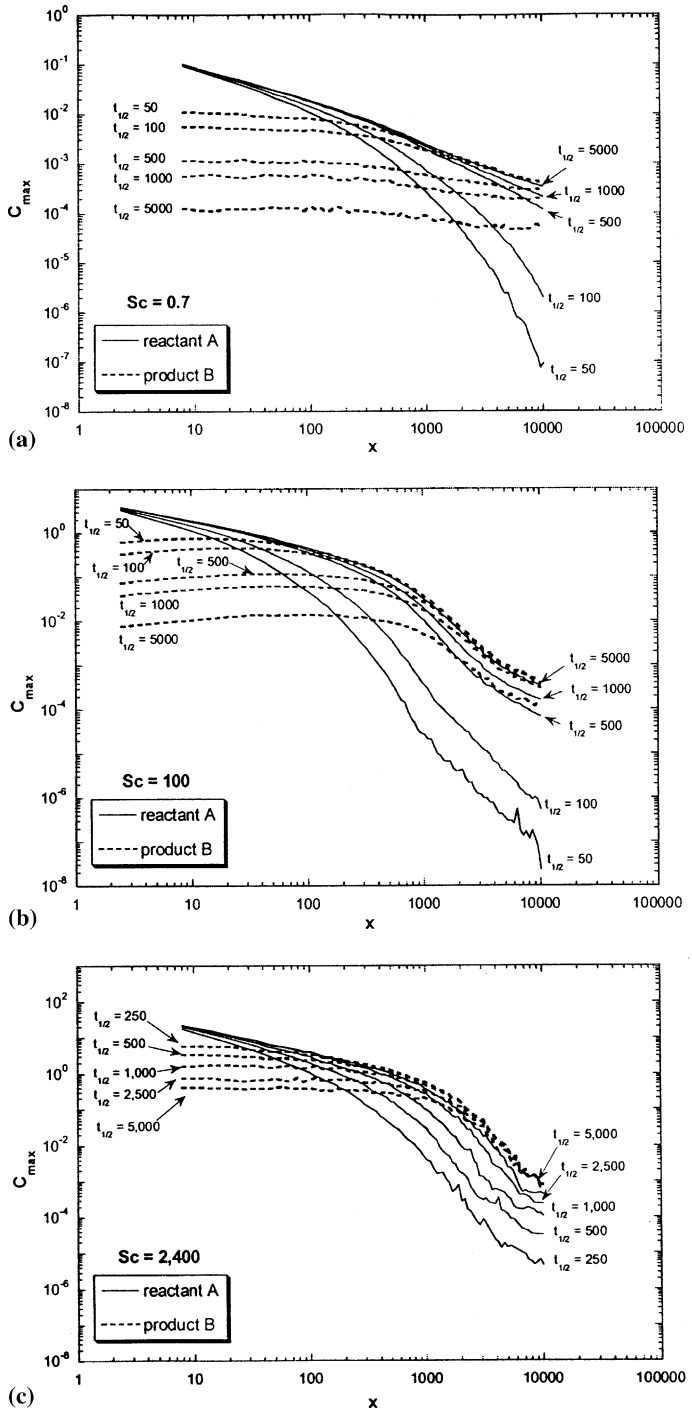

Fig. 8. Ground level concentration of components A and B downstream from a continuous line source for different $t_{1/2}$: (a) $Sc = 0.7$; (b) $Sc = 100$ and (c) $Sc = 2400$.

and 2400, respectively. Results for different rates of reaction, expressed through $t_{1/2}$ are also shown in Fig. 8(a)–(c). As expected, $C_{\max}$ of product B in the x direction is higher for faster reactions. For slow reactions, it

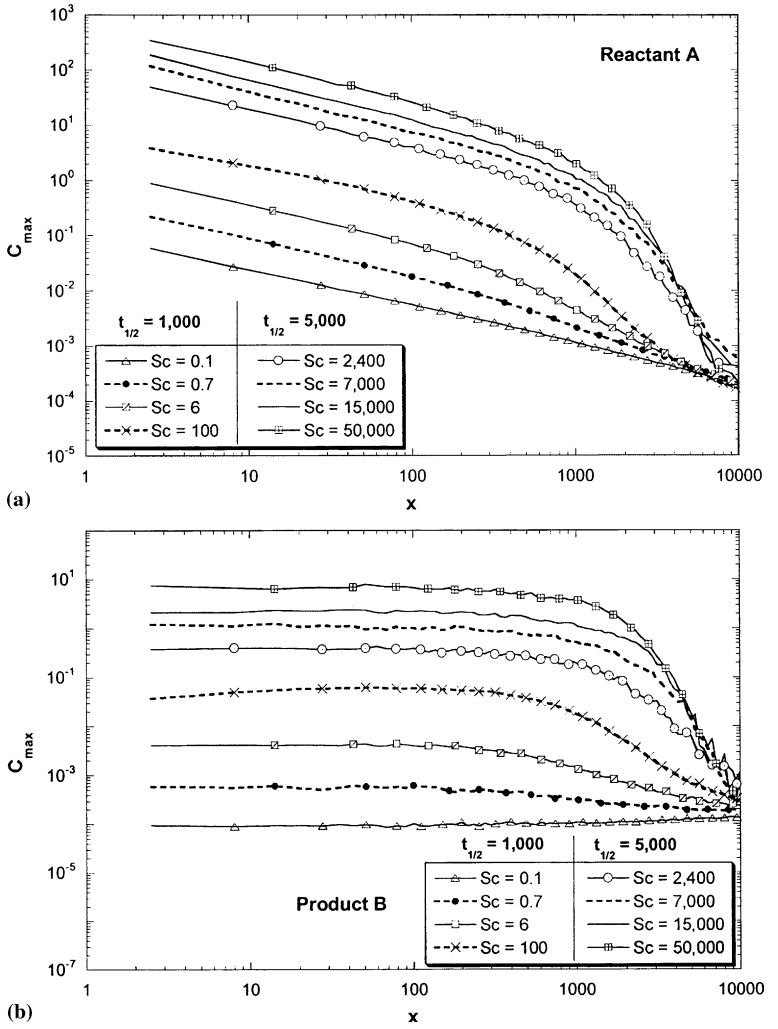

Fig. 9. Ground level concentration downstream from a continuous line source for different Sc and $t_{1/2}$: (a) reactant A and (b) product B.

is higher for reactant A, and this difference is more pronounced for distances farther downstream from the source. Fig. 9(a) and (b) shows $C_{\max}$ as a function of the downstream distance from the source for different Sc for A and B, respectively. The ground-level concentration for the lower Sc number cases ($Sc \leqslant 100$) is presented for $t_{1/2} = 1000$, and for the higher Sc numbers ($Sc \geqslant 2400$) for $t_{1/2} = 5000$. It appears that for product B, a layer with constant $C_{\max}$ is formed at small distances in the streamwise direction. This behavior is also attributed to the fundamental behavior of the plumes as a function of Sc [14]. As Sc increases the first stage of plume development is more pronounced, meaning that more markers A stay close to the wall longer. Markers B are generated from markers A in that region, and those that are generated also stay longer within the wall region. In fact, $C_{\max}$ for B has higher values downstream from the source, rather than right at the source, which is the case for markers A. The different zones of plume development for plumes A and B can still be distinguished, especially for higher Sc numbers.

6.2. Continuous dissolution of the reactant A from the wall of the channel

Fig. 10(a) and (b) shows the mean concentration profiles at the fully developed part of the channel ($x/h > 100$) for a fast and a slow reaction, respectively,

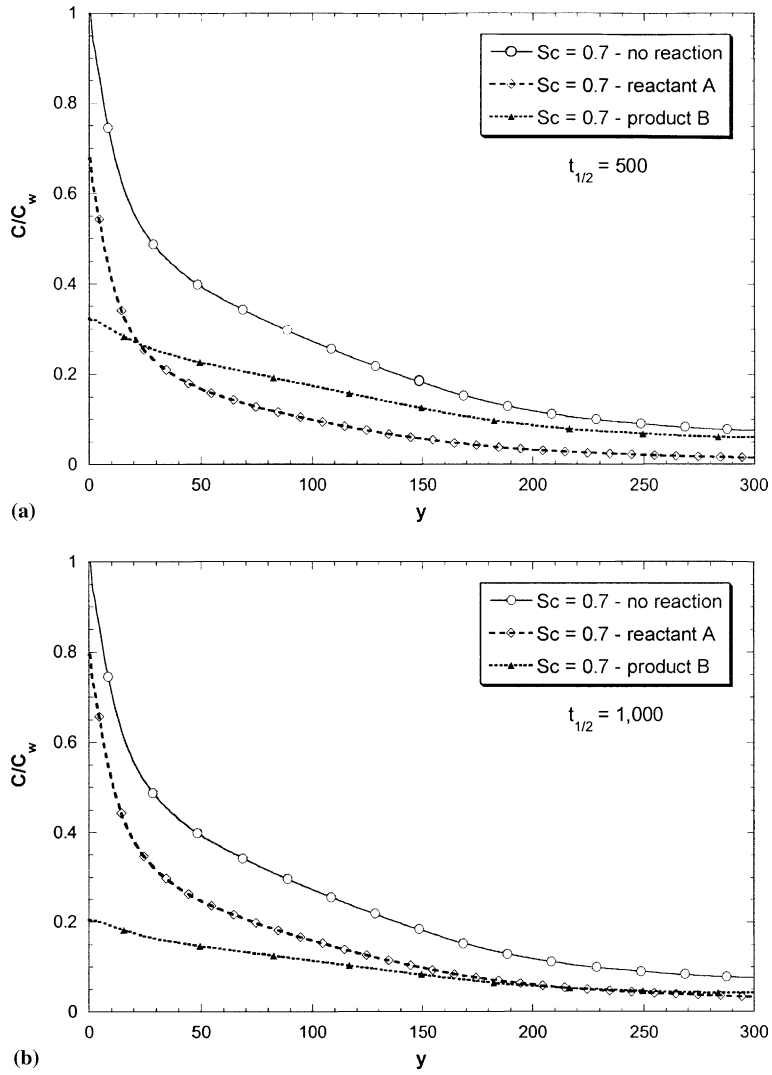

Fig. 10. Mean concentration profiles at the fully developed part of the channel for $Sc = 0.7$: (a) $t_{1/2} = 500$ and (b) $t_{1/2} = 1000$.

for $Sc = 0.7$. The mean concentration profile for the case without reaction is also included for comparison. The mean concentration for each reactant is calculated according to Eq. (5), and then it is made dimensionless using the total concentration at the wall. Since the concentration for each reactant is normalized this way, it is expected that the sum of the concentrations of A and B yields the concentration for the case without reaction, as shown in Fig. 10.

The mass transfer coefficients as a function of the distance downstream from the point at the wall where a constant flux of the reactant A is introduced, are presented in Fig. 11(a) and (b) for various values of $t_{1/2}$ and for the range of Sc. It can be seen that the values for K^+ decrease with the corresponding increase of $t_{1/2}$ and tend asymptotically to the case without reaction (that is, when $t_{1/2} \to \infty$ or $Da \to 0$). A dramatic enhancement of mass transfer due to the chemical reaction is evident, and it is higher for faster reactions (small values of $t_{1/2}$). The enhancement factor, defined as the ratio K^+ (reaction)/K^+ (no reaction), is shown for the cases of $Sc = 0.7$, 100, and 2400 in Fig. 12(a)–(c). As seen, the enhancement factor can increase considerably with increasing downstream distance. The enhancement factor for the fully developed part of the channel is presented in Table 2 for all Sc and $t_{1/2}$ considered in this work. For

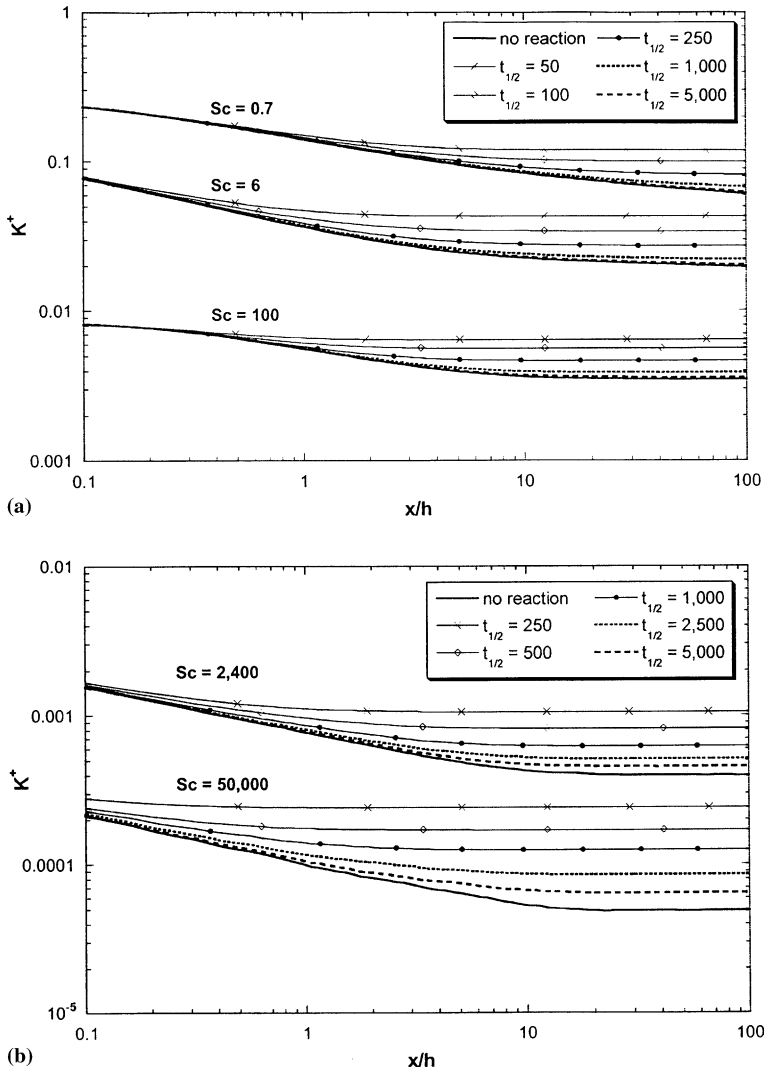

Fig. 11. Mass transfer coefficient for different Sc and $t_{1/2}$ downstream from a step change in mass flux of reactant A from the wall: (a) $Sc = 0.7$, 6, 100 and (b) $Sc = 2400$, 50,000.

example, the mass transfer coefficient for a fast reaction ($t_{1/2} = 50$) can be as much as ten times higher than in the absence of reaction for the case of $Sc = 50,000$.

For very large distances x downstream from the point of step change in mass flux ($x/h > 100$), the concentration profile becomes fully developed for each reaction rate and the concentration gradient in the x direction is constant. In the Lagrangian sense, these are the distances where the mass markers' distribution over the cross-section of the channel does not change with x. Therefore, for a constant driving force (concentration gradient) and constant mass flux, the mass transfer coefficient is also constant for large x, and it is denoted with K_∞^+. Fig. 13 presents K_∞^+ as a function of $t_{1/2}$ for the whole range of Sc examined. Fig. 14 shows the comparison between the fully developed mass transfer coefficients obtained by using available data for different sample sizes (16,129 and 145,161 mass markers). As seen, the agreement is very good, especially for higher values of Sc, which means that the results for $Sc \geqslant 200$ obtained with the fewer number of markers are reliable. The values for K_∞^+ in the absence of reaction are presented for $t_{1/2} = 5 \times 10^4$, since for that case it can be safely assumed that the rate of the reaction is practically zero. Beyond that point ($t_{1/2} \to \infty$), K_∞^+ is independent of $t_{1/2}$, and hence, Eq. (8a) and (8b) can be used to determine the dependence of K_∞^+ on Sc. On the

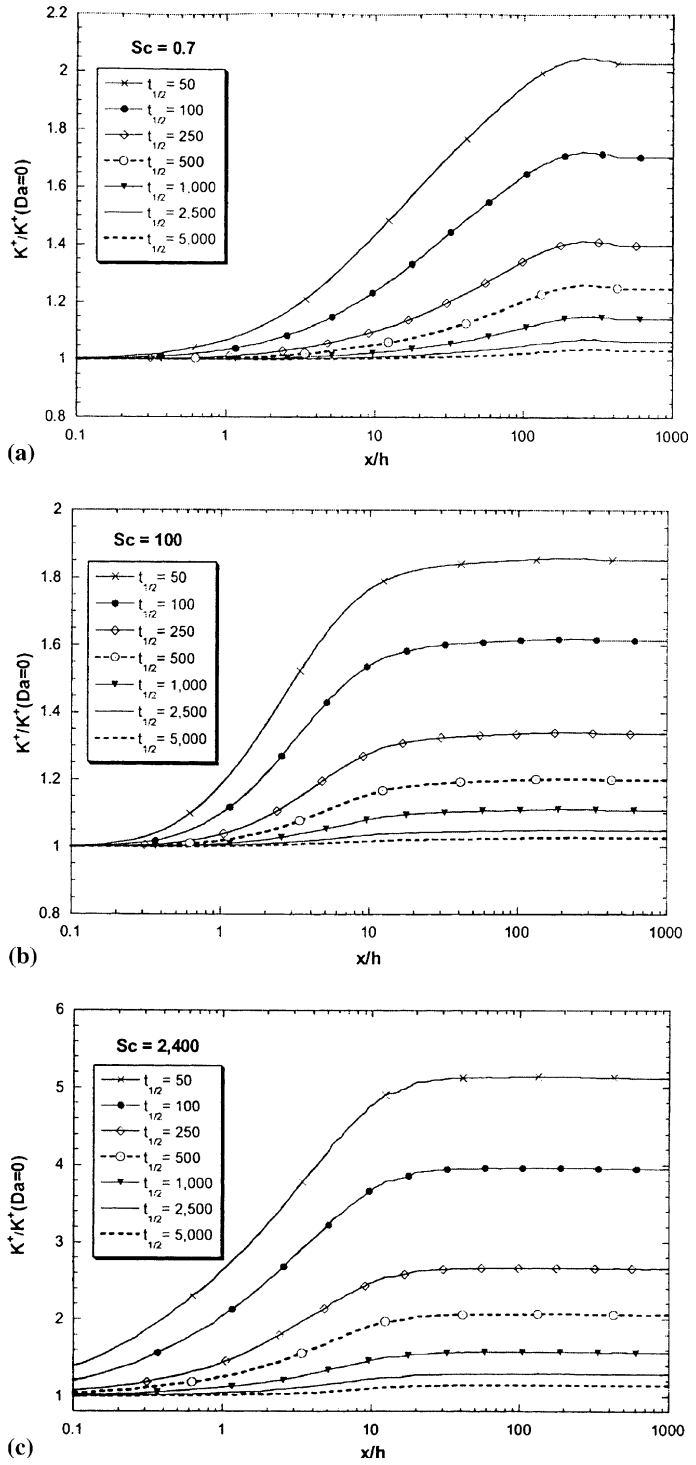

Fig. 12. Mass transfer enhancement factor for different Sc and $t_{1/2}$ downstream from a step change in mass flux of reactant A from the wall: (a) $Sc = 0.7$; (b) $Sc = 100$ and (c) $Sc = 2400$.

other hand, for $t_{1/2} \to 0$, K_{∞}^{+} is evidently a function of $t_{1/2}$ (i.e., the Damköhler number). The following limiting relations for $t_{1/2} \leqslant 250$ are obtained from the data shown in Fig. 13:

Table 2
Enhancement factor, $\phi = K_\infty^+/K_\infty^+(Da=0)$, for different values of the Schmidt number: the half-life time

Sc	$t_{1/2}$						
	50	100	250	500	1000	2500	5000
0.1	2.22	1.83	1.46	1.28	1.16	1.08	1.04
0.7	2.03	1.70	1.40	1.25	1.14	1.07	1.03
6	2.15	1.75	1.39	1.22	1.13	1.06	1.03
10	2.22	1.79	1.41	1.25	1.15	1.08	1.05
100	2.43	2.02	1.59	1.38	1.25	1.16	1.13
200	2.74	2.25	1.73	1.45	1.29	1.18	1.13
500	2.97	2.43	1.81	1.50	1.28	1.13	1.08
2400	5.12	3.94	2.66	2.06	1.57	1.28	1.14
7000	6.47	5.03	3.49	2.59	1.92	1.47	1.24
15,000	8.66	6.39	4.38	3.26	2.34	1.74	1.35
50,000	9.87	7.18	4.92	3.49	2.56	1.75	1.32

$$K_\infty^+(Sc, t_{1/2}\to 0) = 0.2779\cdot Sc^{-0.510} t_{1/2}^{-0.262} \quad \text{for } Sc \leqslant 10 \tag{18a}$$

$$K_\infty^+(Sc, t_{1/2}\to 0) = 0.3662\cdot Sc^{-0.467} t_{1/2}^{-0.400} \quad \text{for } Sc \geqslant 100 \tag{18b}$$

The mass transfer coefficient as a function of k_{A1} and Sc for the whole $t_{1/2}$ range can be found by utilizing the generalized equation proposed by Churchill and Usagi [30] for all phenomena that have different asymptotic behavior at two limits. This generalized equation is of the form

$$\frac{f(w)}{f_\infty(w)} = \left[1+\left(\frac{f_0(w)}{f_\infty(w)}\right)^n\right]^{1/n} \tag{19}$$

where $f_\infty(w)$ and $f_0(w)$ represent asymptotic expressions for large and small values of w. In our case, these functions represent $K_\infty^+(Sc, t_{1/2})$ for large and small values of $t_{1/2}$ expressed through Eqs. (8a), (8b), (18a) and (18b), respectively. Therefore, Eq. (19) becomes

$$\frac{K_\infty^+(Sc, t_{1/2})}{K_\infty^+(Sc, t_{1/2}\to\infty)} = \left[1+\left(\frac{K_\infty^+(Sc, t_{1/2}\to 0)}{K_\infty^+(Sc, t_{1/2}\to\infty)}\right)^n\right]^{1/n} \tag{20}$$

Substitution of Eqs. (8a), (8b), (18a) and (18b) into Eq. (20) yields

$$\phi = \frac{K_\infty^+(Sc, t_{1/2})}{0.0465\cdot Sc^{-0.510}} = \left[1+\left(\frac{5.98}{t_{1/2}^{0.262}}\right)^n\right]^{1/n} \quad \text{for } Sc \leqslant 10 \tag{21a}$$

$$\phi = \frac{K_\infty^+(Sc, t_{1/2})}{0.0835\cdot Sc^{-0.690}} = \left[1+\left(\frac{4.39\cdot Sc^{0.223}}{t_{1/2}^{0.400}}\right)^n\right]^{1/n} \quad \text{for } Sc \geqslant 100 \tag{21b}$$

The exponent n for both equations is determined from statistical analysis by minimizing the mean square errors between the data and the approximations. The best fit with the data is obtained for $n = 5.35$ and $n = 3.0$ for Eqs. (21a) and (21b), respectively. Finally, by using Eqs. (13) and (16), the following expressions are derived for K_∞^+ in terms of Schmidt and Damköhler numbers:

$$K_\infty^+(Sc, Da) = 0.0465\cdot Sc^{-0.51}(1+2.381\times 10^4 Da^{1.4})^{0.187} \quad \text{for } Sc \leqslant 10 \tag{22a}$$

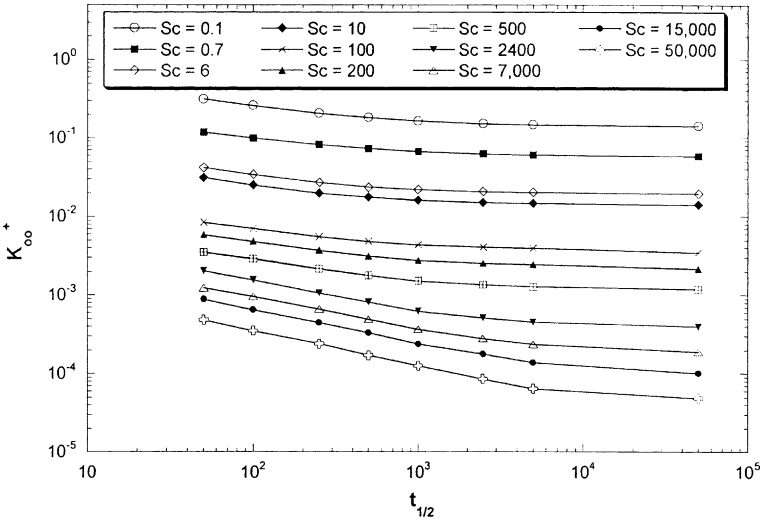

Fig. 13. Mass transfer coefficient for fully developed channel flow as a function of half-life time for different Sc.

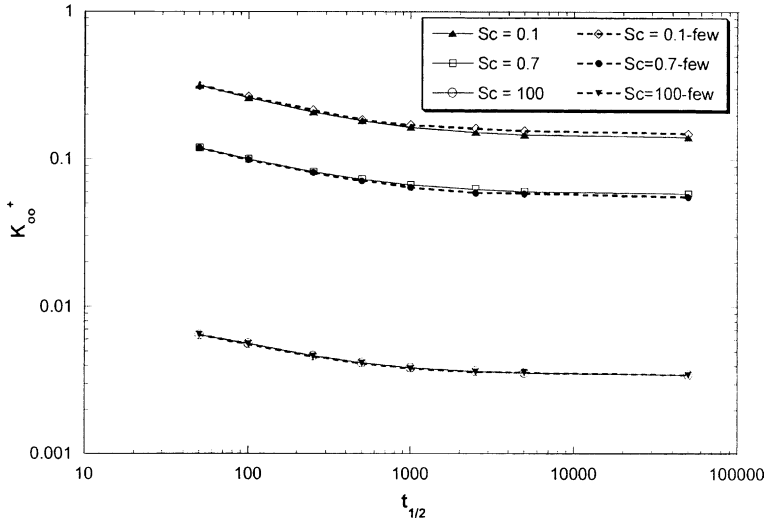

Fig. 14. Effect of marker sample size on the mass transfer coefficient for fully developed channel flow.

$$K^+_\infty(Sc, Da) = 0.0835 \cdot Sc^{-0.69}(1 + 130.5Da^{1.2}Sc^{2/3})^{1/3} \quad \text{for } Sc \geqslant 100 \tag{22b}$$

Fig. 15(a) and (b) presents the fully developed mass transfer coefficient as a function of Sc and Da fitted according to Eqs. (22a) and (22b). It can be seen that both correlations give very good fit with the data for the whole range of Da.

Hanna et al. [6] used a large Schmidt number asymptotic approximation procedure to derive an equation for the enhancement factor in fully developed turbulent flow in a circular tube, which involves a dimensionless reaction rate parameter α, defined as $\alpha = 106.46\gamma(R^+)^{-2}Sc^{1/3}$. Using Eq. (16) and the relations for the characteristic length and time scales, this parameter can be also expressed as $\alpha = 106.46DaSc^{1/3}$. Fig. 16 shows a comparison between the calculated enhancement factor and the enhancement factor presented in [6], as a function of the parameter α. The LST data follow the model for the enhancement factor, but not exactly. The model of Hanna et al. is based on the Reynolds analogy and utilizes the Van Driest formula for the eddy diffusivity close to the wall. However, it has been found both experimentally [31] and computationally using Eulerian DNS [32] that the wall exhibits a "filtering" effect on the turbulence spectrum that contributes to mass transfer (in contrast to the Reynolds analogy that implies that all parts of the velocity spectrum contribute to mass or heat transport). From the Lagrangian point of view, the higher the Sc, the smaller the random molecular jumps in the vertical direction and the harder for turbulence eddies to sweep markers away from the wall. In fact, the higher the Sc, the larger the size (larger wavelength) of eddies that can contribute to turbulent transport close to the wall, and the wavelength threshold is a function of Sc. A closer examination of Fig. 16 shows that the points that do not agree with the Hanna et al. model (mostly $100 \leqslant Sc \leqslant 500$ and $t_{1/2} \leqslant 250$) are the points for which such differences are important. In this range of parameters, one can compare $t_{1/2}$ with the time that it takes for a puff of markers A to get to the second stage of puff transition, $\tau_{\text{zone II}} = 27.1Sc^{0.36}$ (see [23]). For example, $\tau_{\text{zone II}} = 142$ for $Sc = 100$, which means that most markers A react before the puff (and therefore the plume, which is composed by puffs) goes into the second zone of development when $t_{1/2} = 250$. In that case, mass transfer from the wall is between the wall and a puff that is mostly inside the viscous wall sublayer and that is subject to the filtering effect described above.

7. Conclusions

A combined DNS/LST method is used in this work to simulate mass transfer from the wall of a channel and first-order chemical reaction for different values of the Schmidt number and different values of the Damköhler number.

The development of the clouds of the reactant and the product that result from a continuous line source located at the wall of the channel is studied. The behavior of both clouds can be interpreted from a Lagrangian point of view when the behavior of a cloud of contaminants without reaction is taken into account.

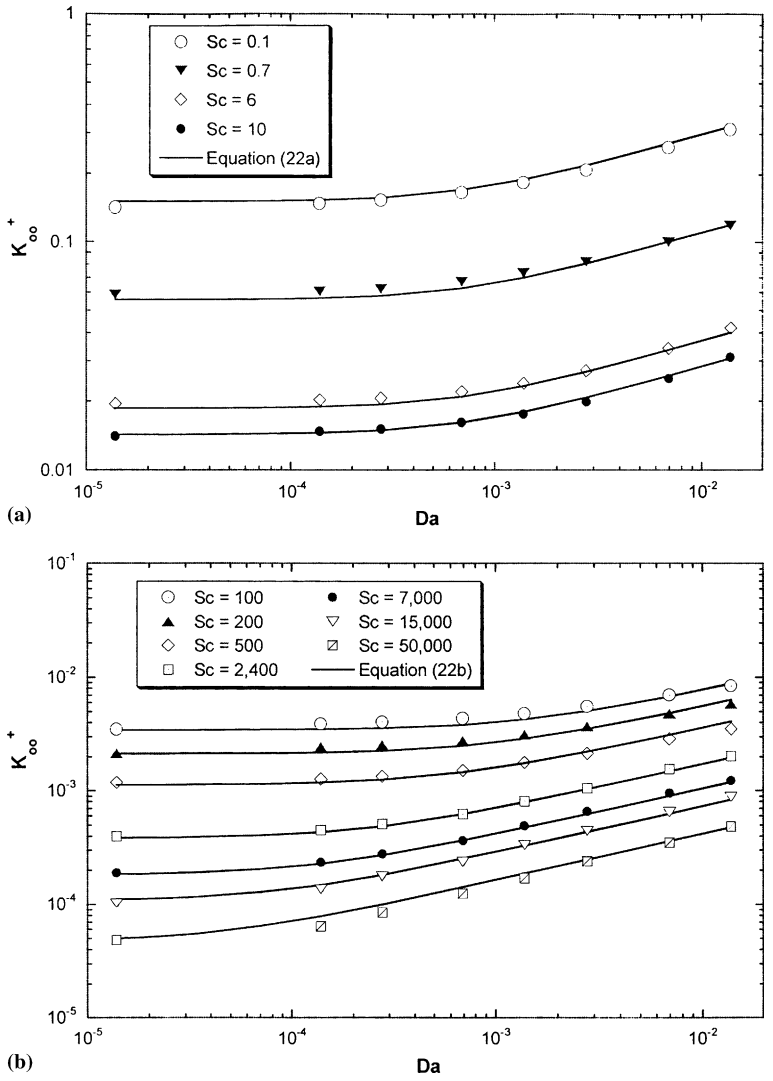

Fig. 15. Comparison of LST data with predictive correlations for the calculation of the mass transfer coefficient as a function of *Sc* and *Da*: (a) low *Sc* and (b) high *Sc*.

The ground level concentration for the reactant exhibits the regions of plume development that have been observed when no reaction occurs, albeit modified as the *Da* changes. The ground level concentration of the product exhibits a region where it is almost constant, due to the fact that the reaction occurs when the reactant markers reside within the viscous wall sublayer, so that it takes longer for the plume of the product to extend in the outer region of the flow.

The effects of the reaction on the mass transfer properties for the dissolution of the reactant from the wall is also examined. It is found that the mass transfer coefficient is enhanced by up to an order of magnitude, depending on *Sc* and *Da*. Two correlations between the mass transfer coefficient and *Da* are proposed, one for low *Sc* and one for high *Sc*. The correlation for high *Sc* presents particular interest, because it provides some insights to turbulent mass transfer from the wall when compared with previously developed models that assume a complete analogy between momentum and mass transfer. A Lagrangian interpretation of the dependence of mass transport properties on molecular properties and on the reaction time scale is provided. This interpretation reduces the case of constant mass flux of a reactant from the wall to the fundamental behavior of an instantaneous line source of reactant at the wall, and the stages of development of the resulting puff relative to the reaction time scale.

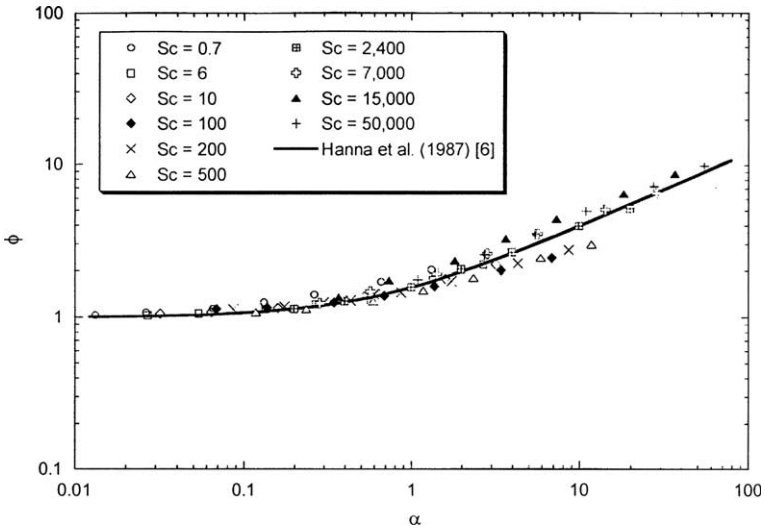

Fig. 16. Comparison of LST data with the model of Hanna et al. [6].

Acknowledgements

The support of NSF under CTS-0209758 is gratefully acknowledged. This work was partially supported by the National Computational Science Alliance under CTS990021N and utilized the NCSA HP/Convex Exemplar SPP-2000 and the NCSA SGI/CRAY Origin2000.

References

[1] M. Chakrabarti, R.M. Kerr, J.C. Hill, Direct numerical simulation of chemical selectivity in homogeneous turbulence, AIChE J. 41 (1995) 2356–2369.
[2] A.D. Leonard, R.C. Hamlen, R.M. Kerr, J.C. Hill, Evaluation of closure models for turbulent reacting flows, Ind. Eng. Chem. Res. 34 (1995) 3640–3652.
[3] M. Chakrabati, J.C. Hill, First-order closure theories for serial–parallel reaction in simulated homogeneous turbulence, AIChE J. 43 (4) (1997) 902–911.
[4] A.D. Leonard, J.C. Hill, Direct numerical simulation of turbulent flows with chemical reaction, J. Scient. Comput. 3 (1998) 25–43.
[5] R.B. Bird, W.E. Stewart, E.N. Lightfoot, Transport Phenomena, Wiley and Sons, New York, 1960, p. 399, 403, 361.
[6] O.T. Hanna, O.S. Sandall, C.L. Wilson, Mass transfer accompanied by first-order chemical reaction for turbulent duct flow, Ind. Eng. Chem. Res. 26 (1987) 2286–2290.
[7] P.G. Saffman, On the effect of the molecular diffusivity in turbulent diffusion, J. Fluid Mech. 8 (1960) 273–283.
[8] T.J. Hanratty, Heat transfer through a homogeneous isotropic turbulent field, AIChE J. 2 (1) (1956) 42–45.
[9] D.V. Papavassiliou, T.J. Hanratty, The use of Lagrangian methods to describe turbulent transport of heat from the wall, Ind. Eng. Chem. Res. 34 (1995) 3359–3367.
[10] D.V. Papavassiliou, T.J. Hanratty, Transport of a passive scalar in a turbulent channel flow, Int. J. Heat Mass Transfer 40 (6) (1997) 1303–1311.
[11] S.S. Ponoth, J.B. McLaughlin, Numerical simulation of mass transfer for bubbles in water, Chem. Eng. Sci. 55 (2000) 1237–1255.
[12] D.V. Papavassiliou, Turbulent transport from continuous sources at the wall of a channel, Int. J. Heat Mass Transfer 45 (17) (2002) 3571–3583.
[13] Y. Mito, T.J. Hanratty, Lagrangian stochastic simulation of turbulent dispersion of heat markers in a channel flow, Int. J. Heat Mass Transfer 46 (6) (2003) 1063–1073.
[14] B.M. Mitrovic, D.V. Papavassiliou, Transport properties for turbulent dispersion from wall sources, AIChE J. 49 (5) (2003) 1095–1108.
[15] S.L. Lyons, T.J. Hanratty, J.B. McLaughlin, Direct numerical simulation of passive heat transfer in a turbulent channel flow, Int. J. Heat Mass Transfer 34 (4/5) (1991) 1149–1161.
[16] A. Guenther, D.V. Papavassiliou, M.D. Warholic, T.J. Hanratty, Turbulent flow in a channel at low Reynolds number, Exper. Fluids 25 (1998) 503–511.
[17] K. Kontomaris, T.J. Hanratty, J.B. McLaughlin, An algorithm for tracking fluid particles in a spectral simulation of turbulent channel flow, J. Computat. Phys. 103 (1993) 231–242.
[18] A. Einstein, Uber die von der molekular-kinetischen theorie der Warme geforderte Bewegung von in ruhenden Flussigkeiten suspendierten Teilchen, Ann. Phys. 17 (1905) 549.
[19] K. Kontomaris, T.J. Hanratty, Effect of molecular diffusivity on point source diffusion in the center of a numerically simulated turbulent channel flow, Int. J. Heat Mass Transfer 37 (13) (1994) 1817–1828.
[20] B.M. Mitrovic, P.M. Le, D.V. Papavassiliou, On the Prandtl or Schmidt number dependence of the turbulence heat or mass transfer, Chem. Eng. Sci. (2002) (under review).

[21] J.E. Cermak, Lagrangian similarity hypothesis applied to diffusion in turbulent shear flow, J. Fluid Mech. 15 (1963) 29–64.
[22] B.A. Kader, Temperature and concentration profiles in fully turbulent boundary layers, Int. J. Heat Mass Transfer 29 (9) (1981) 1541–1544.
[23] D.V. Papavassiliou, Scalar dispersion from an instantaneous line source at the wall of a turbulent channel for medium and high Prandtl number fluids, Int. J. Heat Fluid Flow 23 (2) (2002) 161–172.
[24] D.A. Shaw, T.J. Hanratty, Turbulent mass transfer rates to a wall for large Schmidt numbers, AIChE J. 23 (1) (1977) 28–37.
[25] C.A. Petty, A statistical theory for mass transfer near interfaces, Chem. Eng. Sci. 30 (1975) 413–418.
[26] A.S. Monin, A.M. Yaglom, Statistical Fluid Mechanics: Volume 1, Mechanics of Turbulence, The MIT Press, Cambridge MA, 1965, pp. 279–282.
[27] J.S. Son, T.J. Hanratty, Limiting relation for the eddy diffusivity close to a wall, AIChE J. 13 (1967) 689.
[28] S.W. Churchill, A reinterpretation of the turbulent Prandtl number, Ind. Eng. Chem. Res. 41 (25) (2002) 6393–6401.
[29] R.V. Hogg, E.A. Tanis, Probability and Statistical Inference, 3rd ed., Macmillan Publishing Co, New York, 1988, p. 131.
[30] S.W. Churchill, R. Usagi, A general expression for the correlation of rates of transfer and other phenomena, AIChE J. 18 (1972) 1121–1127.
[31] J.A. Campbell, T.J. Hanratty, Turbulent velocity fluctuations that control mass transfer to a solid boundary, AIChE J. 29 (1983) 215–221.
[32] Y. Na, T.J. Hanratty, Limiting behavior of turbulent scalar transport close to a wall, Int. J. Heat Mass Transfer 43 (10) (2000) 1749–1758.